ACS APPLIED ENERGY MATERIALS

www.acsaem.org Article

Unexpected Enhancement of Molecular n-Doping Efficiency in Polymer Thin Films by a Degradation Product

Francesca Pallini, Sara Mattiello, Marco Cassinelli, Pietro Rossi, Sara Mecca, Wen Liang Tan, Mauro Sassi, Guglielmo Lanzani, Christopher R. McNeill, Mario Caironi,* and Luca Beverina*

Cite This: *ACS Appl. Energy Mater.* 2022, 5, 2421−2429 Read Online

ACCESS | Metrics & More | Article Recommendations | Supporting Information

ABSTRACT: Molecular doping of conjugated polymers is extremely desirable to control charge density gradients and shape the electric field across polymer electronic devices, including highly efficient organic solar cells. It is also a fundamental requirement for organic thermoelectrics and a powerful strategy to boost charge injection and transport properties in transistors. Yet, currently available doping approaches are far from offering a suitable level of control, particularly in the case of n-type doping. We here reveal that part of this limitation lies in the lack of understanding of dominant factors in doping efficiency. In particular, we highlight the key role played by very small amounts of a specific decomposition product formed during processing of the widely used molecular dopant 4-(2,3-dihydro-1,3-dimethyl-1H-benzimidazol-2-yl)-*N*,*N*-dimethylbenzenamine (DMBI-H) in influencing the n-type conductivity in polymer blends. We show that such an overlooked decomposition product acts as a nucleating agent for a new crystalline phase of DMBI-H, with the overall effect of boosting the electrical conductivity of the final doped polymer films. Such results, confirmed by control experiments performed with a different nucleating agent, focus on the crucial role played by the solid-state microstructure in molecular doped semiconductors and offer ground for a significant change in design guidelines for molecular doping strategies.

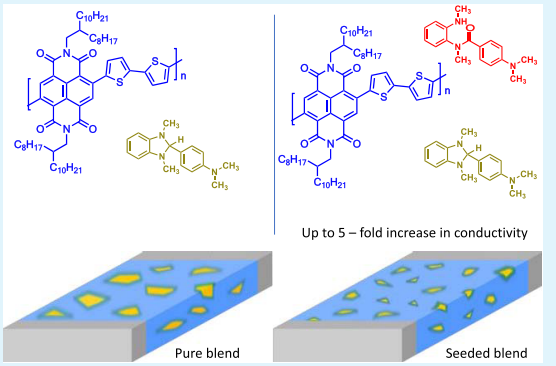

KEYWORDS: *molecular doping, organic semiconductors, plastic electronics, stability, polymer blends*

INTRODUCTION

The development of molecular doping has a major impact on boosting the performances of nearly all plastic (opto)electronic devices.[1] The capability to tune the conductivities of both p- and n-type-doped organic semiconductors over orders of magnitude, while at the same time improving energy-level alignments between different organic materials and metallic contacts, proved to be groundbreaking for vacuum-processed organic light-emitting diodes (OLEDs), organic field-effect transistors (OFETs), and organic photovoltaic (OPV) devices.[2−5] More recently, the same approach demonstrated also critically improved performances in the more challenging solution-processed OPVs[6−9] and organic thermoelectric generators (OTEGs).[10−15] Key to the success of the approach was the development of p- and n-dopants having a broad application window encompassing most of the already developed, high-mobility polymeric, and small-molecule materials.[3,16−18] The p-type doping of hole-transporting semiconductors is energetically simpler due to the relatively high-lying highest occupied molecular orbital (HOMO) levels of materials like polythiophenes. Fluorinated tetracyanoquinodimethane derivatives like F4TCNQ can be handled in air and provide very efficient p-type doping in solution and in solid state.[19,20] The n-type-doped organic semiconductors are more challenging. Suitable dopants should feature HOMO levels higher than −3.8 eV, the energy more or less corresponding to the lowest unoccupied molecular orbital (LUMO) level of high-electron-mobility semiconductors like [6,6]-phenyl C_{61} butyric acid methyl ester ($PC_{60}BM$) or poly{[*N*,*N*′-bis(2-octyldodecyl)-naphthalene-1,4,5,8-bis(dicarboximide)-2,6-diyl]-alt-5,5′-(2,2′-bithiophene)} (P(NDI2OD-T2), Figure 1a).[21−25] This clearly poses serious problems of air stability, not only for the doped polymer but also for the dopant itself. A valuable approach to overcome this problem is the development of kinetically air-stable dopant precursors, which, after incorporation into the host material, can be thermally or photochemically converted in more reductive species through bond formation/cleavage. DMBI-H (Figure 1a) is by far the most widely studied "masked" dopant, particularly in the emerging field of OTEGs.[24,26−28] *Per se*, DMBI-H is a fairly electron-rich molecule (HOMO energy level at −4.4 eV), yet

Received: December 13, 2021
Accepted: January 13, 2022
Published: January 27, 2022

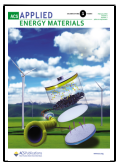

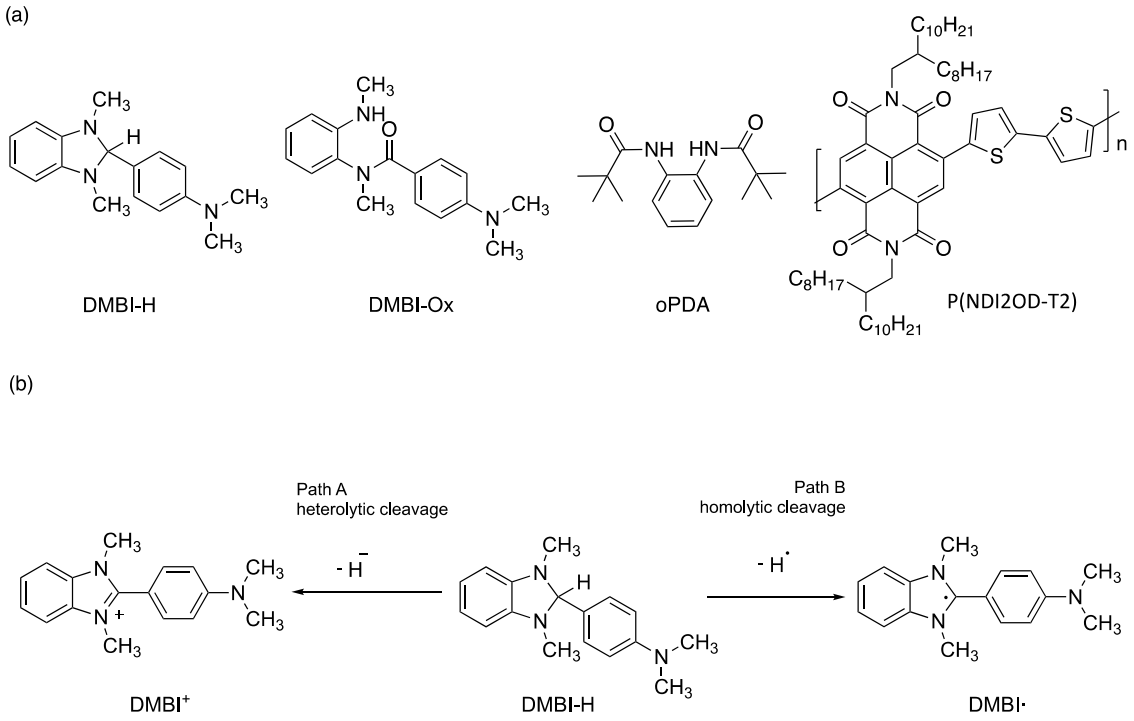

Figure 1. (a) Chemical structures of the molecular dopant DMBI-H, its main decomposition product DMBI-Ox, the nucleating agent oPDA, and the n-type polymer P(NDI2OD-T2). (b) Possible cleavage mechanisms of DMBI-H, with the formation of different reducing species: hydride (heterolytic cleavage, path A) and DMBI$^{\bullet}$ radical (homolytic cleavage, path B).

Scheme 1. Literature Routes toward the Synthesis of DMBI-H (in black) and Improved Synthesis of Amine 3 and DMBI-H Proposed in This Work (in Green)

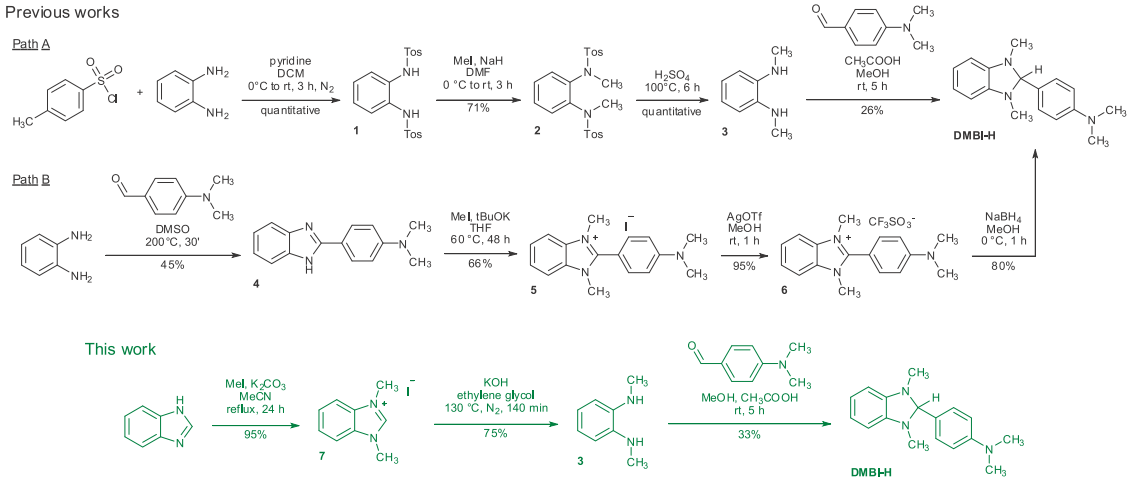

still energetically incapable of doping neither $PC_{60}BM$ (LUMO level at −3.9 eV) nor P(NDI2OD-T2) (LUMO level at −3.8 eV).[29]

The details of the doping mechanism upon which DMBI-H donates one electron to an organic semiconductor are very much dependent upon the specific counterpart. In a series of very detailed papers, Marder and Bao convincingly demonstrated that the doping process in the case of fullerene derivatives is triggered by the donation of a hydride from DMBI-H, with the formation of the DMBI$^+$ cation (Figure 1b, path A). In other cases, the hydride donation is competitive with the homolytic cleavage of the C−H bond and the formation of a highly electron-rich carbon-centered radical, having a SOMO typically placed around −2.40 eV and thus fully capable of n-type doping essentially all organic semiconductors (Figure 1b, path B).[30]

Yi very recently disclosed that the energetics for the heterolytic (hydride donation) and homolytic (hydrogen donation) C−H bond cleavage for the isolated molecule are essentially the same. Conversely, either one of the two competing processes can become dominant, when assisted by the target n-dopable semiconductor. The specific chemical nature of the semiconductor and the details of the interaction geometry determine the preferential pathway.[26,29,31,32]

Regardless of the details of the doping mechanism(s), the two main attractive features generally attributed to DMBI-H are generality and air stability. The former is demonstrated, but the latter is questionable. Very recently, Wang and Demadrille,

https://doi.org/10.1021/acsaem.1c03893
ACS Appl. Energy Mater. 2022, 5, 2421−2429

among others, disclosed the limited stability of DMBI-H while dissolved in organic solvents, including those commonly employed for processing.[33−35] Such observation is somewhat surprising as it is apparently conflicting with the fact that most authors carry out doping experiments in air with commercially available samples of DMBI-H and without mentioning specific purification and/or preliminary characterizations.[27,36−39]

In this paper, we reveal the impact of known concentrations of the DMBI-H degradation byproduct in blends with P(NDI2OD-T2). To do so, we characterized the evolution over time of the nuclear magnetic resonance (NMR) spectra of solutions of carefully purified samples of DMBI-H, prepared in the deuterated analogue of the processing solvent. We characterized and isolated the most relevant byproduct thus formed, confirming the amide structure (DMBI-Ox, Figure 1a).[34,35] Our findings show that the presence of very small amounts of DMBI-Ox triggers the nucleation of DMBI-H in a new crystalline phase with the effect of sizably improving performances, particularly at low doping levels. We interpret the unexpected behavior as seeded crystallization of DMBI-H in very small crystallites within P(NDI2OD-T2). To substantiate this hypothesis, we tested a series of P(NDI2OD-T2) blends with an electrochemically inert nucleating agent, o-phenylenediaminebispivaloylamide (oPDA, Figure 1a). We show that the presence of oPDA enables a 2- to 5-fold increase in the blend electrical conductivity with respect to control experiments having the same dopant concentration. What we report offers the ground for rethinking molecular doping strategies of semiconducting polymers, approached so far only as optimization of a binary system, but revealing itself as a ternary problem in the relevant case of n-type doping based on benzimidazole derivatives.

SYNTHESIS AND PURIFICATION OF DMBI-H

DMBI-H is an established and commercially available molecular dopant. Scheme 1 shows that the literature approaches for its synthesis are straightforward but require several steps, limiting yield and sustainability. The most popular route starts from *N*,*N*′-dimethyl-1,2-phenylenediamine **3**.[27,29] The latter is commercially available but rather expensive and prone to oxidative degradation. 1,2-Phenylenediamine is converted into the corresponding sulfonanilide **1** by reaction with tosyl chloride in dichloromethane (DCM). The deprotonation of **1** in dimethylformamide (DMF), followed by alkylation with methyl iodide, gives product **2**. Hydrolysis in concentrated sulfuric acid at a high temperature, followed by neutralization, gives **3** after chromatographic purification. The final step in the preparation of DMBI-H is the acid-catalyzed condensation between **3** and 4-(dimethylamino)benzaldehyde. The process is in some cases described to be assisted by ultrasound. DMBI-H precipitates and is collected by filtration (Scheme 1, path A). The overall yield is just above 18%. Alternatively, it is possible to react directly 1,2-phenylenediamine with 4-(dimethylamino)benzaldehyde to give the 2-arylbenzimidazole **4** in moderate yield. The same gives iodide **5** after double alkylation with methyl iodide under alkaline conditions, later converted into the corresponding triflate **6** by metathesis with the corresponding silver salt.[40] This intermediate finally gives the desired final product after treatment with $NaBH_4$ with an overall yield of almost 23%.

The main advantage of pathway B is the possibility to change the substitution pattern on the benzimidazole residue using alkylating agents other than methyl iodide. If it were not for the expensiveness of **3**, path A would be preferable. We thus developed an alternative synthesis of **3**, more respectful of atom economy, and improved the subsequent condensation. As it is shown in Scheme 1, inexpensive benzimidazole can be alkylated in an essentially quantitative yield with methyl iodide/K_2CO_3 to give iodide **7**. High-temperature alkaline hydrolysis of **7** affords **3** in 75% yield after vacuum distillation. To the best of our knowledge, the preparative application of such a protocol is original.[28] The usual acid-catalyzed condensation gives analytically pure DMBI-H, after a short silica gel filtration. The overall yield of the protocol is still around 24%, but the improvements in atom economy and waste reduction are very significant.

During purification, we realized how delicate DMBI-H is in solution, especially under a standard laboratory atmosphere. This finding prompted us to challenge the numerous reports describing the pretended ambient stability of DMBI-H, particularly when dissolved in chlorinated solvents.

CHARACTERIZATION OF DMBI-H STABILITY

Pure DMBI-H is a pale yellow crystalline solid that darkens upon storage in air. Commercial samples might be already significantly darkened at first opening. In our experience, pure samples kept under argon and in the dark can be stored for months without hints of degradation, but samples left under laboratory atmosphere darken in a few days (see the Supporting Information). As already observed by Wang, the scenario changes significantly when the dopant is in solution.[34] Being interested in the degradation kinetics under the exact experimental conditions used for processing, we monitored the evolution of a 10 mg/mL solution in d_5-chlorobenzene (deuterated analogue of the most common solvent used in doping experiments) by room-temperature ^{1}H NMR both under argon atmosphere (sample Ar) and under standard laboratory atmosphere (sample O_2). Such a study was necessary to evaluate the composition of solutions used in doping experimental campaigns often requiring a few days to be complete.

The degradation in air is fast and leads to the formation of two products: the amide DMBI-Ox (90 mol %) already isolated by Demadrille[35] and the cation $DMBI^+$ (10 mol %). The mechanistic details of the degradation process are not fully clear, but the far higher stability of the sample prepared under Ar confirms that molecular oxygen plays a role. As it is shown in Figure 2B, after 2 days, the O_2 sample is already 50% decomposed while the Ar one is still barely showing appreciable evolution. Later, even the Ar sample decomposed, likewise because of the reaction with O_2 traces in the glovebox (O_2 and H_2O concentrations, respectively, in the 1−5 and 0.1−0.5 ppm levels during the experiment). In principle, the decomposition of DMBI-H could be due to a reaction with both oxygen and water; we thus repeated the experiment using deuterated chlorobenzene saturated with deuterated water. As it is shown in Figure 1B, the presence of water (orange trace) significantly slows down the degradation kinetics. There could be different explanations for such a phenomenon. On the one side, the presence of water could stabilize one or more of the charged intermediates that Demadrille hypothesized, thus slowing down the reaction.[35] Conversely, water could react with one of the transient species, again leading to more stable intermediates. Without any further mechanistic evidence, it suffices to say that the degradation products with and without water are the same and that the presence of a certain level of

https://doi.org/10.1021/acsaem.1c03893
ACS Appl. Energy Mater. 2022, 5, 2421−2429

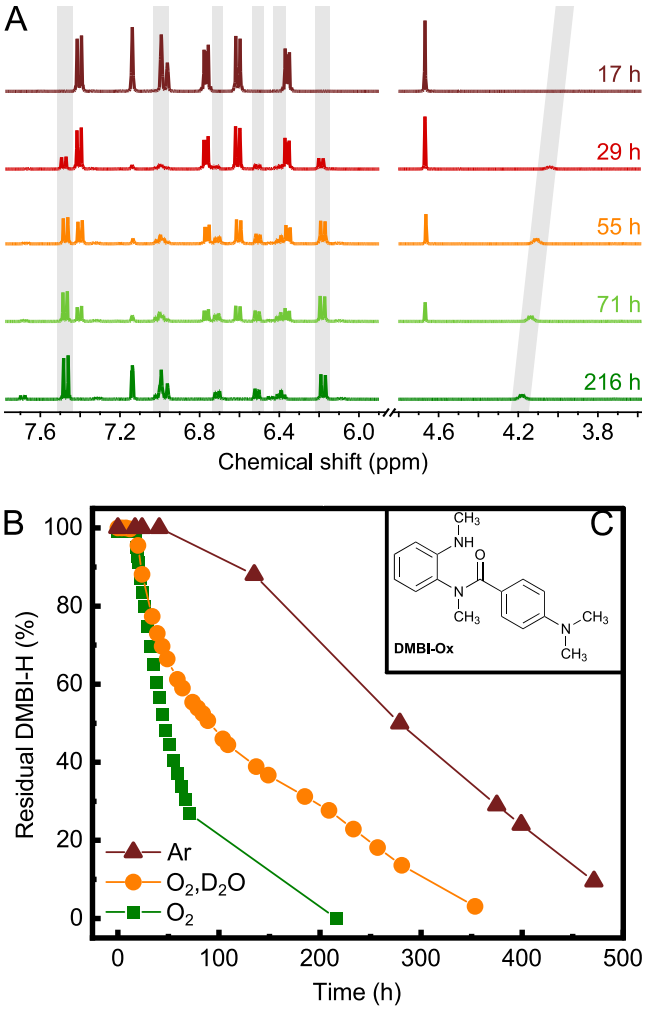

Figure 2. (A) Time evolution of the ^{1}H NMR spectra of a solution of DMBI-H in d_5-chlorobenzene under laboratory atmosphere. Peaks at 6.96, 6.99, and 7.14 ppm are solvent residual signals. Gray rectangles highlight the peaks of the forming species DMBI-Ox. (B) Degradation over time of DMBI-H in d_5-chlorobenzene estimated by ^{1}H NMR for a sample prepared under laboratory atmosphere in the presence (orange circles) and absence (green squares) of deuterated water and under Ar (dark red triangles). The inset (C) shows the structure of the principal identified degradation product, DMBI-Ox.

moisture in the environment somewhat stabilizes DMBI-H solutions in chlorinated solvents.

Our quantitative data complement and confirm those reported in the literature, demonstrating that DMBI-Ox is produced in non-negligible amounts during the timespan normally necessary for sample handling in doping experiments.[35] Nonetheless, DMBI-H has been used successfully under a variety of experimental conditions with comparable performances.[27,36−39]

To explicitly investigate the role played by DMBI-Ox in influencing the electrical properties of DMBI-H-doped polymers, we performed a series of comparative tests using DMBI-H samples aged for progressively increasing time and compared the results with control samples intentionally contaminated with known quantities of DMBI-Ox.

ELECTRICAL CHARACTERIZATION OF DMBI-H/P(NDI2OD-T2) BLENDS

We prepared blends of DMBI-H/P(NDI2OD-T2) at 1, 3, 5, 10, and 30 wt % compositions, all of which dissolved at identical polymer concentrations in chlorobenzene under an inert atmosphere in the glovebox. The samples were stored under conditions identical to those of the NMR-Ar previously discussed, and at precise time intervals, thin films were made by spin coating and thermally annealed under the same conditions (see the Supporting Information). We thus compared electrical conductivity (σ) values as a function of time and dopant concentration (Figure 3). The dopant

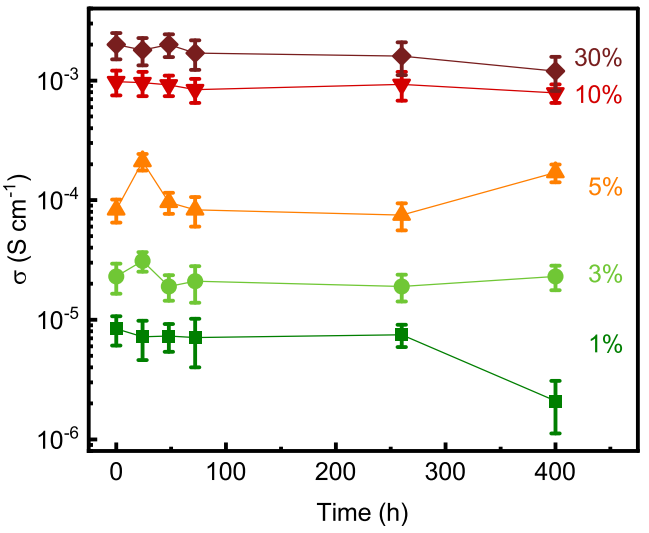

Figure 3. Electrical conductivity as a function of the aging time for DMBI-H/P(NDI2OD-T2) blends of different compositions (from 1 to 30 wt %).

concentration dependence was very much in line with our previous experience with DMBI-H/P(NDI2OD-T2) blends.[27] On the contrary, the time dependence was unexpected. For the first 250 h of aging, we did not monitor any decrease in the conductivity. Only after 400 h, some weak variations are measurable, but the only obvious decrease concerns the 1 wt % sample.

According to the decomposition kinetics we measured (Figure 2A,B), after 250 h of aging in the glovebox, half of the DMBI-H originally dissolved should be decomposed, and yet no effect is apparent from the electrical data. Of course, the assumption that the new samples behave identically to the NMR one, irrespectively of the presence of the polymer, might be totally off target. We thus prepared a sample intentionally contaminated with an amount of DMBI-Ox even larger than that expected to be contained in the 250 h aged sample. In detail, we doped P(NDI2OD-T2) at a 10 wt % level with a 4:1 molar ratio mixture of DMBI-Ox and DMBI-H, corresponding to an active DMBI-H concentration of 2 wt %. According to the data in Figure 3, the corresponding conductivity value is expected to be within 9×10^{-6} S/cm recorded for the 1 wt % doped sample and 2×10^{-5} S/cm obtained for the 3 wt % sample. Instead, we obtained 9×10^{-4} S/cm, a value almost 2 orders of magnitude higher than expected, and consistent with the conductivity of blends containing a 10 wt % amount of pure DMBI-H. According to such data, the net impact of the formation of DMBI-Ox is an improvement rather than a

https://doi.org/10.1021/acsaem.1c03893
ACS Appl. Energy Mater. 2022, 5, 2421−2429

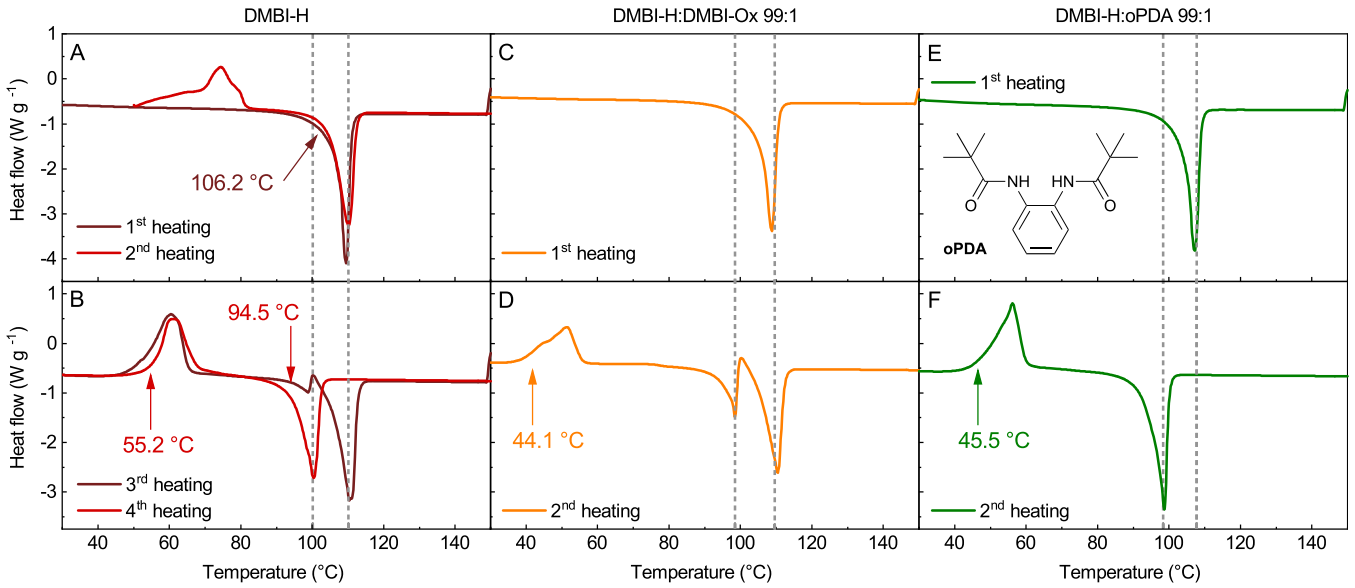

Figure 4. DSC plots for successive heating cycles of a DMBI-H sample (A, B), a DMBI-H:DMBI-Ox 99:1 sample (C, D), and a DMBI-H:oPDA 99:1 sample (E, F). The inset of (E) shows the structure of the oPDA nucleating agent. Measurements carried out at 10 °C/min heating rate and under N_2 flux. Arrows point at the onset of the respective phase transition. Gray dashed lines are a guide to the eye.

decrease in conductivity. DMBI-Ox, an oxidation product of DMBI-H, is not expected to contribute to the doping process directly. We performed a cyclic voltammetry characterization of such derivative, leading to a HOMO level of −5.15 eV (see Figure S9), a value that makes the electron transfer to the polymer not energetically feasible. Nonetheless, we performed a control experiment using a 30 wt % blend of DMBI-Ox/P(NDI2OD-T2). After the standard thermal treatment, we obtained a conductivity of 6×10^{-6} S/cm, still a very small value yet an order of magnitude higher than the 3×10^{-7} S/cm given by pure P(NDI2OD-T2). As conductivity is the product of mobility and carrier density, such an increase could be independent of doping phenomena. Indeed, mobility in polymers as P(NDI2OD-T2) is known to be influenced by the degree of crystallinity.[41] Regardless of the origin, the influence of DMBI-Ox alone on conductivity is too small to explain the results shown in Figure 3. The effect must thus be related to a cooperative effect of both DMBI-H and DMBI-Ox.

DMBI-H is poorly miscible with P(NDI2OD-T2); indeed, the improvement of the mutual compatibility between n-type semiconductors and DMBI-like molecules represents a recognizable trend in the dedicated literature.[22,27,42] There is also a general consensus that, because of the limited interface area between dopants domains and polymer matrix, only a fraction of the dopant molecules can efficiently dope the polymers and contribute to the increase in the conductivity.[43] DBMI-Ox is far less soluble than DMBI-H. Its presence during solvent evaporation could trigger the heterogeneous nucleation of smaller domains of DMBI-H, possibly even promoting the formation of new crystalline phases. The consequent enhancement of the interphase area between dopant and polymer could explain the improved doping efficiency and thus conductivity. To prove such a hypothesis, we performed a detailed thermal analysis of DMBI-H/DMBI-Ox blends.

THERMAL CHARACTERIZATION OF DMBI-H/DMBI-OX BLENDS

Differential scanning calorimetry (DSC) can give insight into the nature of the DMBI-H/DMBI-Ox interaction and helps shedding light on our surprising results. Figure 4A,B shows the thermograms we obtained by repeatedly melting and solidifying an analytically pure sample of DMBI-H. We carried out the experiments under N_2 flux and at a heating rate of 10 °C/min. The cooling curves are omitted as no transition was evident in all of the cases. The first scan, carried out between 25 and 150 °C, shows only the sharp peak associated with the melting of DMBI-H at 108 °C. The second scan shows an exothermic peak at 74 °C, associated with cold crystallization of the sample, followed again by fusion at a slightly higher temperature of 109 °C. In the third heating cycle, the cold crystallization peak shifts at 60 °C and a new sharp endothermic peak appears at 98 °C, followed by the fusion of DMBI-H at 109 °C. In the fourth run, the exothermic crystallization peak is unchanged, but the only endothermic peak still visible is the one at 99 °C, while the original one at 109 °C is no longer visible. Suspecting a role played by thermally induced formation of DMBI-Ox, we first tested by ^{1}H solution NMR if the first heating cycle does induce the formation of DMBI-Ox. As it is shown in Figure S7, peaks associated with the DMBI-Ox impurity are indeed visible at a concentration that increases with the number of thermal cycles. We then prepared a sample having a DMBI-H/DMBI-Ox 99:1 molar composition using carefully purified materials, and we compared the obtained DSC results. As observable in Figure 4C, in the first scan, the thermogram is identical to that of pure DMBI-H, as expected, given that pure DMBI-Ox melts at 170 °C (see the Supporting Information). In the second scan (Figure 4D), the thermogram of the blend features the cold crystallization exothermic peak—in this case at 52 °C—and both the endothermic peaks at 99 and 109 °C. The behavior is very similar to that observed in the third scan of pure DMBI-H. The first-order endothermic transition observed at 99 °C is the melting of a new phase that could be related to two distinct

https://doi.org/10.1021/acsaem.1c03893
ACS Appl. Energy Mater. 2022, 5, 2421−2429

phenomena: (a) the formation of a eutectic mixture between DMBI-Ox and DMBI-H or (b) the seeded crystallization of a different polymorph of pure DMBI-H. On the basis of the thermal characterization alone, a clear-cut assignment is not possible. We thus performed an XRD analysis of carefully purified DMBI-H (Figure 5B), and we compared the results

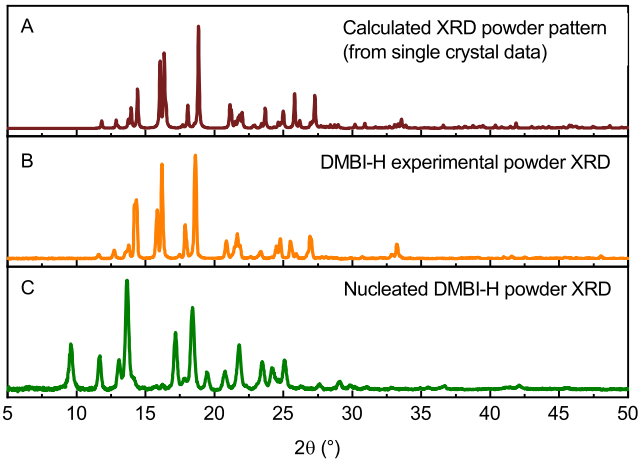

Figure 5. XRD patterns: (A) calculated DMBI-H diffraction powder obtained from the single-crystal data.[35] (B) Experimental pure DMBI-H powder diffraction. (C) Powder diffraction of DMBI-Ox nucleated DMBI-H.

with the calculated XRD pattern obtained starting from the single-crystal data recently published by Demadrille.[35] The two plots are essentially identical, thus confirming that the crystalline phase of the pure materials we obtained by solvent evaporation was the same as that previously described in the literature. We then prepared a sample by heating at 140 °C under N_2 atmosphere a 3 mol % mixture of DMBI-Ox in DMBI-H. At such a temperature, DMBI-H melts and a homogeneous liquid phase forms.

We let the sample cool down to room temperature (the process required about 20 min), obtaining an amorphous glass. Thermal annealing at 60 °C prompted the formation of crystals that we recovered and analyzed by XRD and NMR. While the NMR spectrum still showed essentially pure DMBI-H (see Supporting Information Figure S8), with ∼3% DMBI-Ox, the XRD pattern (Figure 5C) was sizably different, thus confirming the formation of a new polymorph seeded by DMBI-Ox.

ROLE OF NUCLEATING AGENTS IN DMBI-H/P(NDI2OD-T2) BLENDS

To further explore the role of nucleation seeds in influencing the morphology of DMBI-H/polymer blends, we replaced DMBI-Ox with oPDA (Figure 1A)—a very simple nucleating agent soluble in the processing solvent—and we repeated the DSC characterization, while keeping constant the ratio between DMBI-H and impurity. As visible in Figure 4F, the oPDA/DMBI-H blend has a second scan thermogram essentially identical to that we obtained for the fourth scan of pure DMBI-H. We observed the exothermic seeded crystallization at 50 °C (slightly lower than the 52 °C recorded in the case of the DMBI-Ox-containing sample) and the sharp endothermic melting at 98 °C. The melting temperature of the new phase, as obtained in the presence of DMBI-Ox vs oPDA, is essentially identical. The observed shift toward lower temperatures of the onset of the cold crystallization exotherm (from 55 °C of pure DMBI-H to 44−45 °C of the blend) also supports the hypothesis of an increasingly efficient heterogeneous nucleation as such characteristic (more commonly observed on the cooling scan) is a literature-accepted way to compare the efficiencies of different nucleating agents.[44,45]

The remarkable analogy in the behavior of oPDA and DMBI-Ox as contaminants in DMBI-H is also mirrored in the results of electrical characterization. Table 1 summarizes the

Table 1. Electrical Properties of oPDA:DMBI-H/P(NDI2OD-T2) Blends as a Function of the Respective Composition

entry	oPDA:DMBI-H (mol/mol)	wt %	conductivity (S/cm)	enhancement[a]
1	pure oPDA	30	1.5×10^{-6}	
2	80:20	10	1.1×10^{-3}	
3	1:99	3	8.3×10^{-5}	3.6
4	1:99	5	3.9×10^{-4}	4.7
5	1:99	10	3.1×10^{-3}	3.2
6	1:99	30	5×10^{-3}	2.5
7[b]	1:99	5	9.2×10^{-5}	
8[b]	1:99	10	9.5×10^{-4}	
9[b]	1:99	30	1.8×10^{-3}	

[a]Calculated as the ratio with respect to a DMBI-H/P(NDI2OD-T2) blend having the same wt % concentration of pure DMBI-H. [b]Annealed at 90 °C instead of 150 °C.

results we obtained while measuring the electrical conductivity of a series of oPDA:DMBI-H/P(NDI2OD-T2) blends we prepared, thermally annealed, and characterized under conditions identical to those employed for DMBI-H stability campaign. First, we tested (entry 1) a 30 wt % oPDA blend in the polymer obtaining a conductivity of 1.5×10^{-6} S/cm. This value is like that obtained for the 30 wt % DMBI-Ox blend and is likely connected to the same effect. We then tested (entry 2) a 10 wt % concentration of a 4:1 molar mixture of oPDA:DMBI-H, obtaining a conductivity of 1.1×10^{-3} S/cm. The value is again in staggering agreement with the one we obtained using DMBI-Ox under the very same (molar) concentration(9×10^{-4} S/cm).

According to the DSC data, a 1 mol % amount of oPDA over DMBI-H is enough to achieve efficient nucleation of the new phase. We consequently used a 99:1 mixture in the doping of P(NDI2OD-T2), and we compared the results obtained at the very same DMBI-H concentration, but in the absence of oPDA.

In all of the cases, we obtained a clear boosting effect on the electrical conductivity values, particularly evident for the 3 wt % (entry 3) and 5 wt % (entry 4) samples achieving 4- and 5-fold enhancements, respectively. The 30 wt % sample gave a conductivity of 5×10^{-3} S/cm, which is among the highest ever reported under similar experimental conditions for the DMBI-H/P(NDI2OD-T2) system. The observed conductivity enhancement could be attributed to an improved charge mobility, an increased doping efficiency, or both. To understand if the presence of the nucleating agent imparts any change in P(NDI2OD-T2) crystallinity, we performed GIWAXS analysis on P(NDI2OD-T2)/DMBI-H-annealed films, both in the absence and presence of oPDA (Figure 6A,B, respectively). P(NDI2OD-T2) adopts face-on orienta-

https://doi.org/10.1021/acsaem.1c03893
ACS Appl. Energy Mater. 2022, 5, 2421−2429

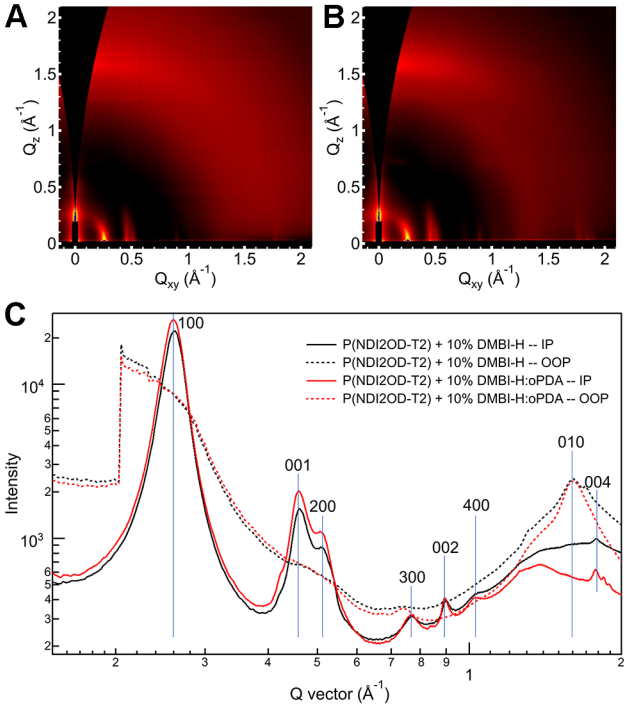

Figure 6. (A) 2D grazing-incidence wide-angle X-ray scattering (GIWAXS) patterns of the P(NDI2OD-T2) film doped with 10 wt % of DMBI and (B) GIWAXS pattern of the P(NDI2OD-T2) film doped with 10 wt % of the DMBI:oPDA 99:1 mixture. (C) Sector-averaged 1D profiles along OOP (dashed line) and IP (full lines).

tion in both films, as evidenced by the presence of in-plane (IP) (*h*00) lamellar stacking peaks, IP (001) backbone repeat peaks, and out-of-plane (OOP) $\pi-\pi$ stacking peaks in the sector-averaged profiles. Very weak OOP (*h*00) lamellar stacking peaks indicate minority edge-on orientation. The measurements showed no noticeable differences in the polymer crystallinity in the two samples, indicating that the presence of oPDA does not alter the molecular packing within the ordered polymer phase. Such an observation is in favor of a more efficient doping process, rather than an enhanced carrier mobility. As a further confirmation of the role played by heterogeneous nucleation, we repeated 5, 10, and 30 wt % tests reducing the annealing temperature at 90 °C. Under such conditions, the nucleation of the new phase is not possible as this would require melting of DMBI-H at 110 °C. Consistently, the conductivity values we observed are essentially identical to those obtained with pure DMBI-H. Figure 7 shows a cartoon highlighting the proposed role of DMBI-Ox in influencing the microstructure of the blend.

CONCLUSIONS

Summing up the results of our electrical/thermal combined characterization, we can conclude that the formation of DMBI-Ox during handling of DMBI-H at a low concentration does not negatively affect the electrical conductivity of the blend. On the contrary, once realized the very peculiar role played by DMBI-Ox in the complex ternary blend, it is even possible to exploit its presence to enhance performances. We believe that our findings significantly change the design guidelines for new doping strategies involving DMBI-H-like compounds and *n*-type polymers like P(NDI2OD-T2). Rather than focusing exclusively on increasing the mutual miscibility of the two

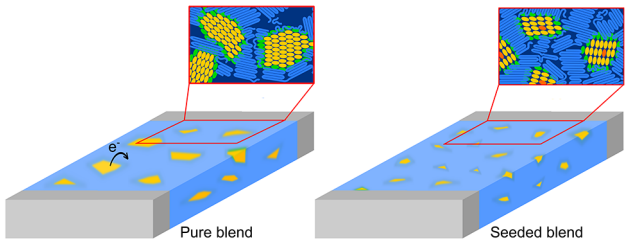

Figure 7. Cartoon highlighting the proposed role of DMBI-Ox in influencing the microstructure of P(NDI2OD-T2)/DMBI-H blends. Left: DMBI-H (yellow) forms domains within the structure of the semicrystalline polymer (blue). The green lines show the heterojunction between dopant and polymer, where doping happens. Right: the presence of DMBI-Ox (red dots) triggers the nucleation of DMBI-H in smaller domains pertaining to the heterogeneously nucleated new phase highlighted by the DSC traces.

components, a characteristic helping doping efficiency but negatively affecting charge carrier mobility, attention should be focused on the solid-state microstructure of such blends and the nature of the phases and interphases involved. Indeed, our data show that the very same dopant can be present in two different phase-segregated forms, one melting at 108−110 °C and the other at 98−99 °C. The data also suggest that nucleation of the latter is strongly enhanced in the presence of nucleating agents in the form of decomposition products (DMBI-Ox) or an exogenous additive (oPDA). Such seeded nucleation appears to have a striking effect on the doping process. Although no conclusion can be currently drawn in this respect, such an observation hints at an interfacial doping mechanism between two different phases rather than on a more simplistic dissolution of the dopant into the polymer phase. In such a scenario, heterogeneous nucleation is expected to play a key role in the extension of phase segregation, microstructure, polymorphism, and reactivity during doping.[46] We believe that our findings—albeit so far limited to the case of DMBI-H in P(NDI2OD-T2)—will prompt a rigorous screening of different nucleating agents, aiming at achieving both higher electrical performances and a deeper understanding of the underlying phenomena in complex blends of polymers and molecular dopants.

ASSOCIATED CONTENT

Supporting Information

The Supporting Information is available free of charge at https://pubs.acs.org/doi/10.1021/acsaem.1c03893.

Materials, and methods, including photographs of the samples; synthetic procedures for all compounds; ^{1}H and ^{13}C NMR characterization of all derivatives; additional experimental details on DMBI-H degradation; additional DSC characterizations; details on electrical characterization; and details on the electrochemical characterization (PDF)

AUTHOR INFORMATION

Corresponding Authors

Mario Caironi − *Center for Nano Science and Technology@PoliMi, Istituto Italiano di Tecnologia, 20133 Milan, Italy;* orcid.org/0000-0002-0442-4439; Email: Mario.Caironi@iit.it

https://doi.org/10.1021/acsaem.1c03893
ACS Appl. Energy Mater. 2022, 5, 2421−2429

Luca Beverina − *Department of Materials Science, Università di Milano-Bicocca, 20125 Milan, Italy;* orcid.org/0000-0002-6450-545X; Email: luca.beverina@unimib.it

Authors

Francesca Pallini − *Department of Materials Science, Università di Milano-Bicocca, 20125 Milan, Italy*

Sara Mattiello − *Department of Materials Science, Università di Milano-Bicocca, 20125 Milan, Italy;* orcid.org/0000-0002-2907-0964

Marco Cassinelli − *Center for Nano Science and Technology@PoliMi, Istituto Italiano di Tecnologia, 20133 Milan, Italy;* orcid.org/0000-0003-1679-5090

Pietro Rossi − *Center for Nano Science and Technology@PoliMi, Istituto Italiano di Tecnologia, 20133 Milan, Italy; Physics Department, Politecnico di Milano, 20133 Milan, Italy*

Sara Mecca − *Department of Materials Science, Università di Milano-Bicocca, 20125 Milan, Italy*

Wen Liang Tan − *Department of Materials Science and Engineering, Monash University, Clayton, VIC 3800, Australia;* orcid.org/0000-0002-0180-3919

Mauro Sassi − *Department of Materials Science, Università di Milano-Bicocca, 20125 Milan, Italy;* orcid.org/0000-0002-5529-6449

Guglielmo Lanzani − *Center for Nano Science and Technology@PoliMi, Istituto Italiano di Tecnologia, 20133 Milan, Italy; Physics Department, Politecnico di Milano, 20133 Milan, Italy;* orcid.org/0000-0002-2442-4495

Christopher R. McNeill − *Department of Materials Science and Engineering, Monash University, Clayton, VIC 3800, Australia;* orcid.org/0000-0001-5221-878X

Complete contact information is available at: https://pubs.acs.org/10.1021/acsaem.1c03893

Author Contributions

The manuscript was written through contributions of all authors. All authors have given approval to the final version of the manuscript.

Notes

The authors declare no competing financial interest.

■ ACKNOWLEDGMENTS

This work was performed in part on the SAXS/WAXS beamline43 at the Australian Synchrotron, part of ANSTO. L.B., M.S., S.M., and F.P. gratefully acknowledge the financial contribution from MIUR under Grants "Dipartimenti di Eccellenza 2017 Project − Materials for Energy" and PRIN2017 BOOSTER (2017YXX8AZ).

■ REFERENCES

(1) Salzmann, I.; Heimel, G. Toward a Comprehensive Understanding of Molecular Doping Organic Semiconductors (Review). *J. Electron Spectrosc. Relat. Phenom.* **2015**, *204*, 208−222.

(2) Zhang, Y.; Zhou, H.; Seifter, J.; Ying, L.; Mikhailovsky, A.; Heeger, A. J.; Bazan, G. C.; Nguyen, T.-Q. Molecular Doping Enhances Photoconductivity in Polymer Bulk Heterojunction Solar Cells. *Adv. Mater.* **2013**, *25*, 7038−7044.

(3) Jacobs, I. E.; Moulé, A. J. Controlling Molecular Doping in Organic Semiconductors. *Adv. Mater.* **2017**, *29*, No. 1703063.

(4) Lin, Y.; Firdaus, Y.; Nugraha, M. I.; Liu, F.; Karuthedath, S.; Emwas, A.; Zhang, W.; Seitkhan, A.; Neophytou, M.; Faber, H.; Yengel, E.; McCulloch, I.; Tsetseris, L.; Laquai, F.; Anthopoulos, T. D. 17.1% Efficient Single-Junction Organic Solar Cells Enabled by N-Type Doping of the Bulk-Heterojunction. *Adv. Sci.* **2020**, *7*, No. 1903419.

(5) Reineke, S.; Lindner, F.; Schwartz, G.; Seidler, N.; Walzer, K.; Lüssem, B.; Leo, K. White Organic Light-Emitting Diodes with Fluorescent Tube Efficiency. *Nature* **2009**, *459*, 234−238.

(6) Yan, H.; Tang, Y.; Sui, X.; Liu, Y.; Gao, B.; Liu, X.; Liu, S. F.; Hou, J.; Ma, W. Increasing Quantum Efficiency of Polymer Solar Cells with Efficient Exciton Splitting and Long Carrier Lifetime by Molecular Doping at Heterojunctions. *ACS Energy Lett.* **2019**, *4*, 1356−1363.

(7) Lin, Y.; Nugraha, M. I.; Firdaus, Y.; Scaccabarozzi, A. D.; Anies, F.; Emwas, A.-H.; Yengel, E.; Zheng, X.; Liu, J.; Wahyudi, W.; Yarali, E.; Faber, H.; Bakr, O. M.; Tsetseris, L.; Heeney, M.; Anthopoulos, T. D. A Simple N-Dopant Derived from Diquat Boosts the Efficiency of Organic Solar Cells to 18.3%. *ACS Energy Lett.* **2020**, *5*, 3663−3671.

(8) Lin, Y.; Firdaus, Y.; Nugraha, M. I.; Liu, F.; Karuthedath, S.; Emwas, A.-H.; Zhang, W.; Seitkhan, A.; Neophytou, M.; Faber, H.; Yengel, E.; McCulloch, I.; Tsetseris, L.; Laquai, F.; Anthopoulos, T. D. 17.1% Efficient Single-Junction Organic Solar Cells Enabled by n-Type Doping of the Bulk-Heterojunction. *Adv. Sci.* **2020**, *7*, No. 1903419.

(9) Jung, M.-C.; Kojima, H.; Matsumura, I.; Benten, H.; Nakamura, M. Diffusion and Influence on Photovoltaic Characteristics of P-Type Dopants in Organic Photovoltaics for Energy Harvesting from Blue-Light. *Org. Electron.* **2018**, *52*, 17−21.

(10) Ail, U.; Jafari, M. J.; Wang, H.; Ederth, T.; Berggren, M.; Crispin, X. Thermoelectric Properties of Polymeric Mixed Conductors. *Adv. Funct. Mater.* **2016**, *26*, 6288−6296.

(11) Jiang, Q.; Sun, H.; Zhao, D.; Zhang, F.; Hu, D.; Jiao, F.; Qin, L.; Linseis, V.; Fabiano, S.; Crispin, X.; Ma, Y.; Cao, Y. High Thermoelectric Performance in N-Type Perylene Bisimide Induced by the Soret Effect. *Adv. Mater.* **2020**, *32*, No. 2002752.

(12) Liu, J.; Ye, G.; Zee, B.; van der Dong, J.; Qiu, X.; Liu, Y.; Portale, G.; Chiechi, R. C.; Koster, L. J. A. N-Type Organic Thermoelectrics of Donor-Acceptor Copolymers: Improved Power Factor by Molecular Tailoring of the Density of States. *Adv. Mater.* **2018**, *30*, No. 1804290.

(13) Liu, J.; Shi, Y.; Dong, J.; Nugraha, M. I.; Qiu, X.; Su, M.; Chiechi, R. C.; Baran, D.; Portale, G.; Guo, X.; Koster, L. J. A. Overcoming Coulomb Interaction Improves Free-Charge Generation and Thermoelectric Properties for n-Doped Conjugated Polymers. *ACS Energy Lett.* **2019**, *4*, 1556−1564.

(14) Xiong, M.; Yan, X.; Li, J.-T.; Zhang, S.; Cao, Z.; Prine, N.; Lu, Y.; Wang, J.-Y.; Gu, X.; Lei, T. Efficient N-Doping of Polymeric Semiconductors through Controlling the Dynamics of Solution-State Polymer Aggregates. *Angew. Chem., Int. Ed.* **2021**, *60*, 8189−8197.

(15) Cassinelli, M.; Cimò, S.; Biskup, T.; Jiao, X.; Luzio, A.; McNeill, C. R.; Noh, Y.-Y.; Kim, Y.-H.; Bertarelli, C.; Caironi, M. Enhanced N-Type Doping of a Naphthalene Diimide Based Copolymer by Modification of the Donor Unit. *Adv. Electron. Mater.* **2021**, *7*, No. 2100407.

(16) Kiefer, D.; Kroon, R.; Hofmann, A. I.; Sun, H.; Liu, X.; Giovannitti, A.; Stegerer, D.; Cano, A.; Hynynen, J.; Yu, L.; Zhang, Y.; Nai, D.; Harrelson, T. F.; Sommer, M.; Moulé, A. J.; Kemerink, M.; Marder, S. R.; McCulloch, I.; Fahlman, M.; Fabiano, S.; Müller, C. Double Doping of Conjugated Polymers with Monomer Molecular Dopants. *Nat. Mater.* **2019**, *18*, 149−155.

(17) Salzmann, I.; Heimel, G.; Oehzelt, M.; Winkler, S.; Koch, N. Molecular Electrical Doping of Organic Semiconductors: Fundamental Mechanisms and Emerging Dopant Design Rules. *Acc. Chem. Res.* **2016**, *49*, 370−378.

(18) Yamashita, Y.; Tsurumi, J.; Ohno, M.; Fujimoto, R.; Kumagai, S.; Kurosawa, T.; Okamoto, T.; Takeya, J.; Watanabe, S. Efficient Molecular Doping of Polymeric Semiconductors Driven by Anion Exchange. *Nature* **2019**, *572*, 634−638.

(19) Pingel, P.; Neher, D. Comprehensive Picture of p-Type Doping of P3HT with the Molecular Acceptor F4TCNQ. *Phys. Rev. B* **2013**, *87*, No. 115209.

(20) Li, J.; Zhang, G.; Holm, D. M.; Jacobs, I. E.; Yin, B.; Stroeve, P.; Mascal, M.; Moulé, A. J. Introducing Solubility Control for Improved Organic P-Type Dopants. *Chem. Mater.* **2015**, *27*, 5765−5774.
(21) Anthony, J. E.; Facchetti, A.; Heeney, M.; Marder, S. R.; Zhan, X. N-Type Organic Semiconductors in Organic Electronics. *Adv. Mater.* **2010**, *22*, 3876−3892.
(22) Liu, J.; Qiu, L.; Alessandri, R.; Qiu, X.; Portale, G.; Dong, J.; Talsma, W.; Ye, G.; Sengrian, A. A.; Souza, P. C. T.; Loi, M. A.; Chiechi, R. C.; Marrink, S. J.; Hummelen, J. C.; Koster, L. J. A. Enhancing Molecular N-Type Doping of Donor-Acceptor Copolymers by Tailoring Side Chains. *Adv. Mater.* **2018**, *30*, No. 1704630.
(23) Werner, A.; Li, F.; Harada, K.; Pfeiffer, M.; Fritz, T.; Leo, K.; Machill, S. N-Type Doping of Organic Thin Films Using Cationic Dyes. *Adv. Funct. Mater.* **2004**, *14*, 255−260.
(24) Kolesov, V. A.; Fuentes-Hernandez, C.; Chou, W.-F.; Aizawa, N.; Larrain, F. A.; Wang, M.; Perrotta, A.; Choi, S.; Graham, S.; Bazan, G. C.; Nguyen, T.-Q.; Marder, S. R.; Kippelen, B. Solution-Based Electrical Doping of Semiconducting Polymer Films over a Limited Depth. *Nat. Mater.* **2017**, *16*, 474−480.
(25) Yan, H.; Chen, Z.; Zheng, Y.; Newman, C.; Quinn, J. R.; Dötz, F.; Kastler, M.; Facchetti, A. A High-Mobility Electron-Transporting Polymer for Printed Transistors. *Nature* **2009**, *457*, 679−686.
(26) Zeng, Y.; Zheng, W.; Guo, Y.; Han, G.; Yi, Y. Doping Mechanisms of N-DMBI-H for Organic Thermoelectrics: Hydrogen Removal vs. Hydride Transfer. *J. Mater. Chem. A* **2020**, *8*, 8323−8328.
(27) Saglio, B.; Mura, M.; Massetti, M.; Scuratti, F.; Beretta, D.; Jiao, X.; McNeill, C. R.; Sommer, M.; Famulari, A.; Lanzani, G.; Caironi, M.; Bertarelli, C. *N* -Alkyl Substituted 1 *H* -Benzimidazoles as Improved n-Type Dopants for a Naphthalene-Diimide Based Copolymer. *J. Mater. Chem. A* **2018**, *6*, 15294−15302.
(28) Naab, B. D.; Zhang, S.; Vandewal, K.; Salleo, A.; Barlow, S.; Marder, S. R.; Bao, Z. Effective Solution- and Vacuum-Processed n-Doping by Dimers of Benzimidazoline Radicals. *Adv. Mater.* **2014**, *26*, 4268−4272.
(29) Naab, B. D.; Guo, S.; Olthof, S.; Evans, E. G. B.; Wei, P.; Millhauser, G. L.; Kahn, A.; Barlow, S.; Marder, S. R.; Bao, Z. Mechanistic Study on the Solution-Phase n-Doping of 1,3-Dimethyl-2-Aryl-2,3-Dihydro-1 H-Benzoimidazole Derivatives. *J. Am. Chem. Soc.* **2013**, *135*, 15018−15025.
(30) Liu, J.; Van der Zee, B.; Villava, D. R.; Ye, G.; Kahmann, S.; Kamperman, M.; Dong, J.; Qiu, L.; Portale, G.; Loi, M. A.; Hummelen, J. C.; Chiechi, R. C.; Baran, D.; Koster, L. J. A. Molecular Doping Directed by a Neutral Radical. *ACS Appl. Mater. Interfaces* **2021**, *13*, 29858−29865.
(31) Zhu, X.-Q.; Zhang, M.-T.; Yu, A.; Wang, C.-H.; Cheng, J.-P. Hydride, Hydrogen Atom, Proton, and Electron Transfer Driving Forces of Various Five-Membered Heterocyclic Organic Hydrides and Their Reaction Intermediates in Acetonitrile. *J. Am. Chem. Soc.* **2008**, *130*, 2501−2516.
(32) Jhulki, S.; Un, H.-I.; Ding, Y.-F.; Risko, C.; Mohapatra, S. K.; Pei, J.; Barlow, S.; Marder, S. R. Reactivity of an Air-Stable Dihydrobenzoimidazole n-Dopant with Organic Semiconductor Molecules. *Chem* **2021**, *7*, 1050−1065.
(33) Hasegawa, E.; Yoshioka, N.; Tanaka, T.; Nakaminato, T.; Oomori, K.; Ikoma, T.; Iwamoto, H.; Wakamatsu, K. Sterically Regulated α-Oxygenation of α-Bromocarbonyl Compounds Promoted Using 2-Aryl-1,3-Dimethylbenzimidazolines and Air. *ACS Omega* **2020**, *5*, 7651−7665.
(34) Yang, C.-Y.; Ding, Y.-F.; Huang, D.; Wang, J.; Yao, Z.-F.; Huang, C.-X.; Lu, Y.; Un, H.-I.; Zhuang, F.-D.; Dou, J.-H.; Di, C.; Zhu, D.; Wang, J.-Y.; Lei, T.; Pei, J. A Thermally Activated and Highly Miscible Dopant for N-Type Organic Thermoelectrics. *Nat. Commun.* **2020**, *11*, No. 3292.
(35) Bardagot, O.; Aumaître, C.; Monmagnon, A.; Pécaut, J.; Bayle, P.-A.; Demadrille, R. Revisiting Doping Mechanisms of N-Type Organic Materials with N-DMBI for Thermoelectric Applications: Photo-Activation, Thermal Activation, and Air Stability. *Appl. Phys. Lett.* **2021**, *118*, No. 203904.
(36) Xiong, M.; Yan, X.; Li, J.; Zhang, S.; Cao, Z.; Prine, N.; Lu, Y.; Wang, J.; Gu, X.; Lei, T. Efficient N-Doping of Polymeric Semiconductors through Controlling the Dynamics of Solution-State Polymer Aggregates. *Angew. Chem.* **2021**, *133*, 8270−8278.
(37) Schlitz, R. A.; Brunetti, F. G.; Glaudell, A. M.; Miller, P. L.; Brady, M. A.; Takacs, C. J.; Hawker, C. J.; Chabinyc, M. L. SolubilityLimited Extrinsic nType Doping of a High Electron Mobility Polymer for Thermoelectric Applications. *Adv. Mater.* **2014**, *26*, 2825−2830.
(38) Liu, J.; Qiu, L.; Alessandri, R.; Qiu, X.; Portale, G.; Dong, J.; Talsma, W.; Ye, G.; Sengrian, A. A.; Souza, P. C. T.; Loi, M. A.; Chiechi, R. C.; Marrink, S. J.; Hummelen, J. C.; Koster, L. J. A. Enhancing Molecular N-Type Doping of Donor-Acceptor Copolymers by Tailoring Side Chains. *Adv. Mater.* **2018**, *30*, No. 1704630.
(39) Gross, Y. M.; Trefz, D.; Dingler, C.; Bauer, D.; Vijayakumar, V.; Untilova, V.; Biniek, L.; Brinkmann, M.; Ludwigs, S. From Isotropic to Anisotropic Conductivities in P(NDI2OD-T2) by (Electro-)Chemical Doping Strategies. *Chem. Mater.* **2019**, *31*, 3542−3555.
(40) Riera-Galindo, S.; Orbelli Biroli, A.; Forni, A.; Puttisong, Y.; Tessore, F.; Pizzotti, M.; Pavlopoulou, E.; Solano, E.; Wang, S.; Wang, G.; Ruoko, T.-P.; Chen, W. M.; Kemerink, M.; Berggren, M.; di Carlo, G.; Fabiano, S. Impact of Singly Occupied Molecular Orbital Energy on the N-Doping Efficiency of Benzimidazole Derivatives. *ACS Appl. Mater. Interfaces* **2019**, *11*, 37981−37990.
(41) Steyrleuthner, R.; Di Pietro, R.; Collins, B. A.; Polzer, F.; Himmelberger, S.; Schubert, M.; Chen, Z.; Zhang, S.; Salleo, A.; Ade, H.; Facchetti, A.; Neher, D. The Role of Regioregularity, Crystallinity, and Chain Orientation on Electron Transport in a High-Mobility n-Type Copolymer. *J. Am. Chem. Soc.* **2014**, *136*, 4245−4256.
(42) Kiefer, D.; Giovannitti, A.; Sun, H.; Biskup, T.; Hofmann, A.; Koopmans, M.; Cendra, C.; Weber, S.; Anton Koster, L. J.; Olsson, E.; Rivnay, J.; Fabiano, S.; McCulloch, I.; Müller, C. Enhanced N-Doping Efficiency of a Naphthalenediimide-Based Copolymer through Polar Side Chains for Organic Thermoelectrics. *ACS Energy Lett.* **2018**, *3*, 278−285.
(43) Schlitz, R. A.; Brunetti, F. G.; Glaudell, A. M.; Miller, P. L.; Brady, M. A.; Takacs, C. J.; Hawker, C. J.; Chabinyc, M. L. Solubility-Limited Extrinsic n-Type Doping of a High Electron Mobility Polymer for Thermoelectric Applications. *Adv. Mater.* **2014**, *26*, 2825−2830.
(44) Treat, N. D.; Nekuda Malik, J. A.; Reid, O.; Yu, L.; Shuttle, C. G.; Rumbles, G.; Hawker, C. J.; Chabinyc, M. L.; Smith, P.; Stingelin, N. Microstructure Formation in Molecular and Polymer Semiconductors Assisted by Nucleation Agents. *Nat. Mater.* **2013**, *12*, 628−633.
(45) Lindqvist, C.; Bergqvist, J.; Feng, C.-C.; Gustafsson, S.; Bäcke, O.; Treat, N. D.; Bounioux, C.; Henriksson, P.; Kroon, R.; Wang, E.; Sanz-Velasco, A.; Kristiansen, P. M.; Stingelin, N.; Olsson, E.; Inganäs, O.; Andersson, M. R.; Müller, C. Fullerene Nucleating Agents: A Route Towards Thermally Stable Photovoltaic Blends. *Adv. Energy Mater.* **2014**, *4*, No. 1301437.
(46) Paulsen, B. D.; Tybrandt, K.; Stavrinidou, E.; Rivnay, J. Organic Mixed Ionic−Electronic Conductors. *Nat. Mater.* **2020**, *19*, 13−26.

https://doi.org/10.1021/acsaem.1c03893
ACS Appl. Energy Mater. 2022, 5, 2421−2429